

## QUANTIFICATION OF CASTING SKIN IN DUCTILE AND COMPACTED GRAPHITE IRONS AND ITS EFFECT ON TENSILE PROPERTIES

D. Stefanescu, S. Wills and J. Massone  
The Ohio State University, Columbus, OH, USA

F. Duncan  
Ashland Casting Solutions, Dublin, OH, USA

Copyright 2008 American Foundry Society

### Abstract

*The mechanical properties of ductile iron (DI) and compacted graphite iron (CGI) are measured and reported on standard machined specimens (as per ASTM). However, most castings retain most of the as-cast surface. This surface layer (the casting skin) includes both surface and subsurface features. Because of the casting skin, the mechanical properties of the part are typically significantly lower than those found on standard ASTM machined specimens.*

*The technical objectives of this research were to identify the individual features that together define skin quality in DI and CGI, to develop a method for the measurement of skin thickness, and to quantify the influence of the skin of thin wall (2 to 6 mm) DI castings on its tensile properties.*

*The features of the casting skin include surface (roughness) and subsurface (graphite degradation, graphite depletion, pearlitic rim) elements. Graphite shape measurements were used to evaluate graphite degradation. Graphite area measurements were used to determine the thickness of the*

*graphite depleted layer. Microhardness measurements are useful when a pearlitic rim occurs. The average thickness of the skin for thin wall DI castings ranged from 0.15 to 0.45mm, while for CGI it ranged from 0.7 to 2.5mm.*

*It was found as expected that the strength decreased with thicker casting skin. The tensile and yield strength skin factor (ratio between the strength of as-cast and machined test plates) was about 0.93. This should be viewed as an upper limit, as only one of the surfaces of the mechanical properties test plate was as-cast. More significant reduction in strength should be expected.*

*Diffusion calculations confirmed that graphite degradation, graphite depletion and the pearlitic rim are the result of magnesium and carbon depletion at the mold/metal interface because of their oxidation. Alternatively, carbon diffusion from the mold can also result in pearlitic rim formation.*

**Keywords:** ductile iron, compacted graphite iron, casting skin, surface quality, tensile properties.

---

### Introduction

The mechanical properties of DI, as those of most metallic materials, are measured on and reported (as per ASTM) on standard machined specimens. However, most castings retain most of the as-cast surface. This surface layer, commonly referred to as the *casting skin*, includes both surface and subsurface, and is typically incorporated in the term *surface quality*. Because of the casting skin, the mechanical properties of the part may be significantly different from those found on the standard ASTM specimens machined from the same casting. It is expected that as the thickness of the casting decreases, the relative effect of the skin on the mechanical properties increases. This issue has received only limited attention<sup>1,2,3</sup>.

Recent research has demonstrated that lightweight DI castings can be produced by reducing the wall thickness. Their static

mechanical properties are fully compatible with ASTM requirements<sup>4</sup>. However, it was also found that, when the tests are performed on non machined samples, and not on the standard fully machined specimens, these properties depend heavily on surface quality. It is therefore important to further investigate the impact of casting skin on the mechanical properties and the machinability of light weight DI castings.

Industrial experience with compacted graphite iron (CGI) motor blocks shows that one of the main defects encountered in these castings is the occurrence of a graphite degradation layer (flake graphite skin). There are no clear solutions for this problem at this time.

The technical objectives of this research work included:

- identification of the individual features that together define skin quality (e.g., surface roughness, subsurface microstructure, subsurface

graphite morphology, microstructure gradient, and microhardness gradient) of DI and CGI;

- development of a method for characterization of skin quality;
- quantification of the influence of the skin of thin wall (2 to 6 mm) ductile iron (TWDI) castings on its tensile properties.

### Literature Background

Goodrich and Lobenhofer<sup>1</sup> showed that there is a tendency towards decreasing the strength and elongation of DI because of the casting skin in the as-cast tensile test sample. They found a larger effect on the smaller castings, and reported different skin quality generated by different molding materials. DI samples cast in chemically bonded sand exhibited a surface layer of about 1.3 mm depth with degenerated graphite shapes and other microstructural anomalies. The matrix microstructure of the surface layer showed a pearlitic matrix, while the bulk of the sample exhibited ferritic-pearlitic matrix.

Dix *et al.*<sup>4</sup> demonstrated that the tensile strength of TWDI is 17% lower on sand-blast as-cast plates as compared with machined plates, and that slight grinding of the surface may result in 13% improvement (Fig. 1). Similar effects were documented by Labreque *et al.*<sup>5</sup>

Mampaey *et al.*<sup>2</sup> studied the influence of the casting skin on gray iron. Fig. 2 shows the change in ultimate tensile strength (UTS) as the diameter of a 20mm sand cast round bar was gradually decreased to 8mm by machining. There is a marked increase in UTS as a layer of about 1 mm is removed from

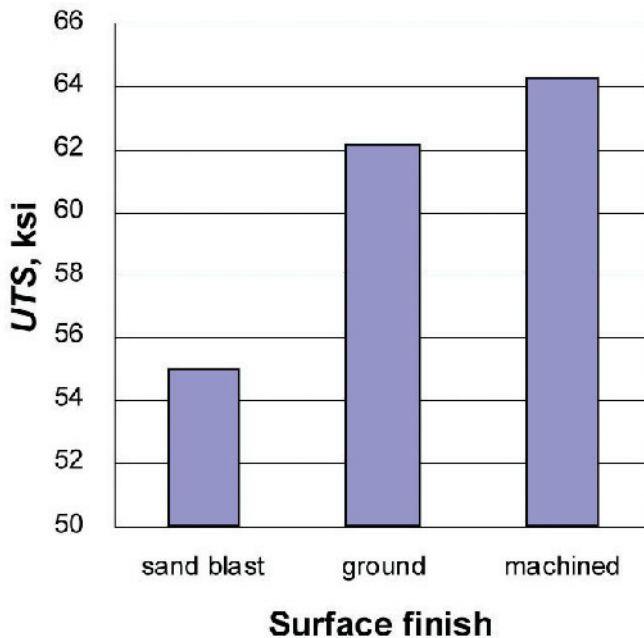


Figure 1. Average tensile strength of TWDI as a function of surface finish.<sup>4</sup>

the sample. It was concluded that the cause of the decrease in strength in the presence of the casting skin was the formation of type D graphite at the surface layer, and, to a lesser extent, the increased ferrite content at the surface. Fig. 3 shows that there is a large amount of D graphite in the subsurface layer. The skin effect on strength was negligible for the lower strength gray irons, while it was of about 20% for a 300 MPa gray iron. Although specific for gray irons, Mampaey's study is useful to exemplify the relevance of the skin quality on iron castings.

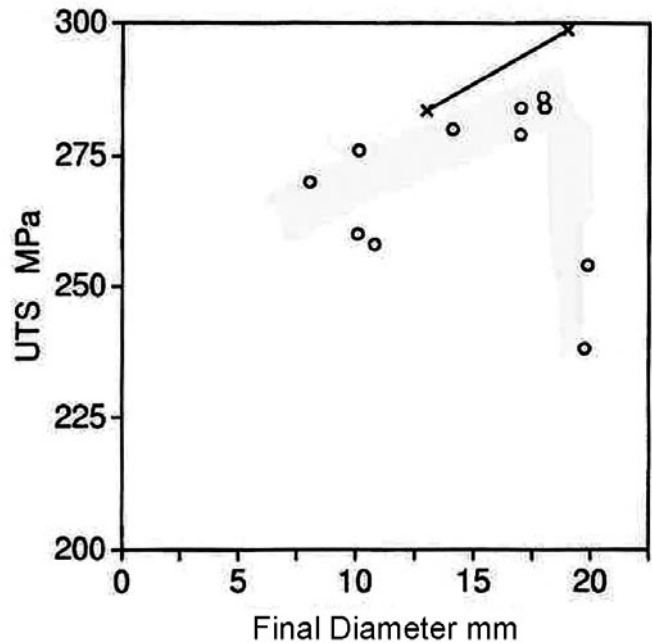


Figure 2. The tensile strength of gray iron as a function of sample diameter. Different diameters are obtained by machining a 20mm sand cast round bar.<sup>2</sup>

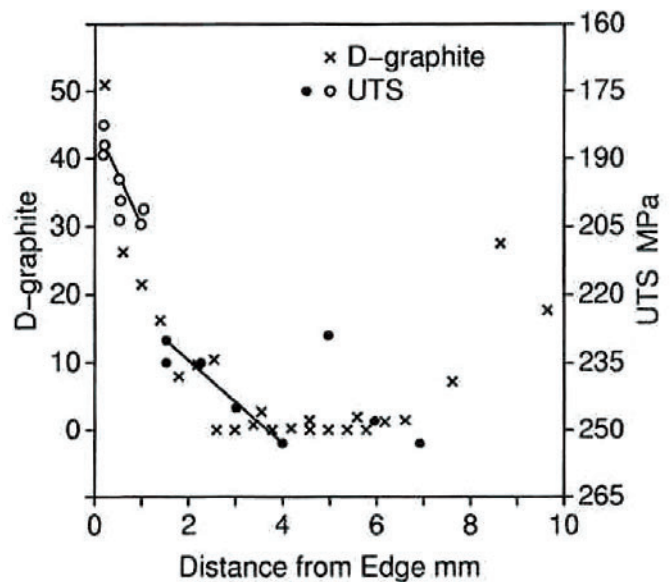


Figure 3. Amount of type-D graphite along the casting radius of a 20mm sand cast round gray iron bar.<sup>2</sup>

Aufderheide *et al.*<sup>6</sup> performed a systematic study on process variables (binder, coating, sand fineness, pouring temperature, and magnesium and inoculation level) that affect the casting skin of TWDI castings. They noted that sand fineness and magnesium level have the higher contributions to the skin effect.

Duncan and Kroker<sup>7</sup> analyzed lamellar graphite skin formation on the surface of CG iron. They concluded that slow cooling rates and small undercooling promote flake graphite growth, and that skin transition is caused by an imbalance between spheroidizing, primary and gaseous elements in the iron composition. The authors suggested that thermal gradient along the specimen height may be responsible for the wedge-shaped formation of skin in the vertical experimental samples.

Since surface finish seems to have such a significant effect on static mechanical properties, it is expected that the effect on fatigue properties will be even more remarkable. Unfortunately there is a paucity of data in the literature. As shown in Fig. 4, a “rough surface” can substantially decrease the fatigue limit<sup>8</sup>. However, the graph does not include any quantification of the surface quality. Labrecque *et al.*<sup>9</sup> concluded from experiments on TWDI (4 and 6 mm thickness) that the fatigue endurance limit (tensile stress) on machined samples is 2 to 19% higher as compared to the results obtained for samples having their as-cast surface exposed to the cyclic stresses.

Because findings of previous research<sup>4</sup> have suggested that there is a roughness threshold above which tensile strength decreases significantly (see Fig. 5), there is a clear need to identify a critical skin quality above which casting properties decrease dramatically.

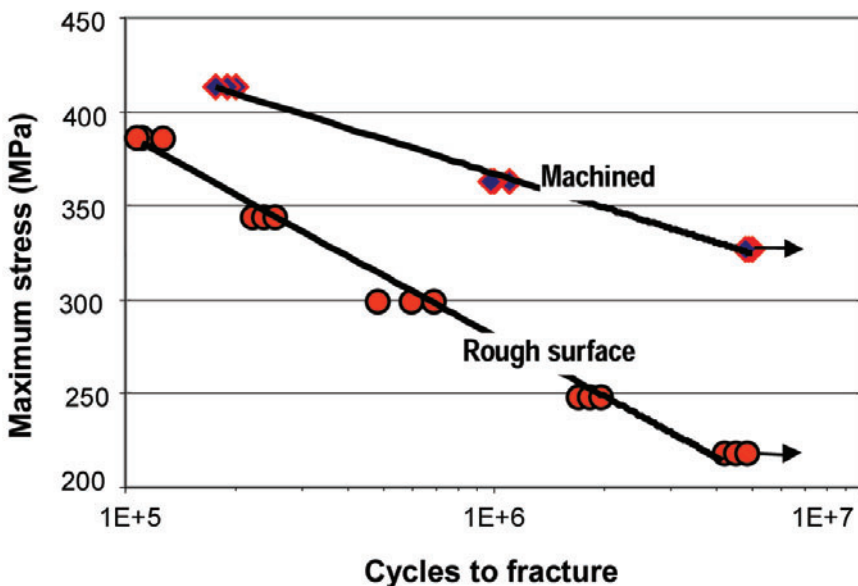


Figure 4. Influence of surface finish on bending fatigue.<sup>8</sup>

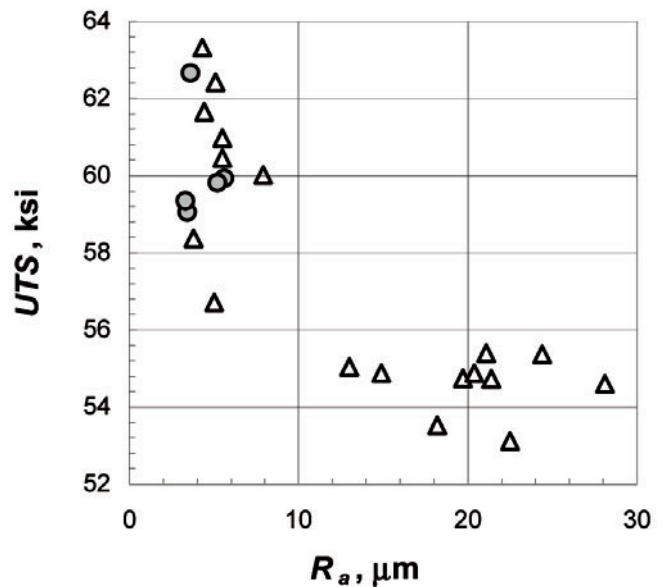


Figure 5. The influence of surface roughness on tensile strength and elongation.<sup>4</sup>

### Skin Quality Definition and Measurement

A preliminary analysis of the factors that may account for the decreased static mechanical properties of TWDI measured on skin-covered specimens resulted in the identification of a number of responsible features:

- The surface roughness may be acting as stress concentrator.
- Surface cracks, other than roughness, may be present at the surface, nucleating fracture.
- Irregular graphite shapes present at the surface, such as compacted or exploded graphite, may account for a weaker skin.
- The matrix microstructure in the subsurface layer may be different than the bulk matrix of the casting (pearlite rim, graphite depletion).

To establish the methodology for skin quality measurement both DI test plates (poured at the Univ. of Alabama) and CGI test coupons (poured at Ashland Inc.) were used. The skin features of interest and the measurements performed in this work for the characterization of these features are presented in Table 1. As the roughness is a surface feature and is not related to the skin thickness (subsurface feature), it was not included in the analysis of these samples.

**Table 1. Skin features and methods for their measurement.**

Skin feature		Measurement
Surface	surface roughness	roughness average
Subsurface	graphite morphology	graphite shape factors
	graphite depletion	graphite area
		graphite count
	subsurface matrix microstructure	pearlite area
microhardness		

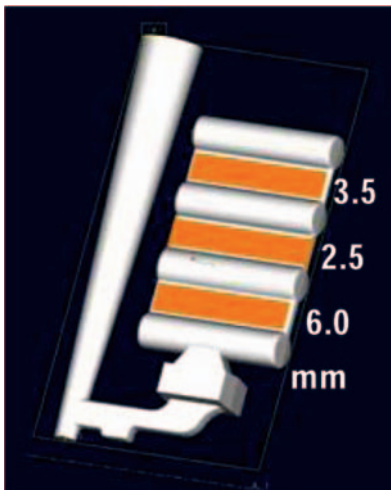


**Figure 6. Vertical plates casting with cylindrical risers.**

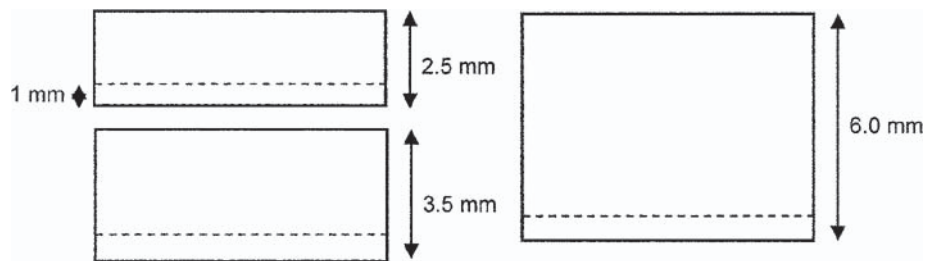


**Figure 7. Schematic of the 2.5, 3.5, and 6mm metallographic samples.**

**Table 2. Quantities measured through image analysis.**

Quantity	Equation	Definitions
Sphericity	$S = 4 \cdot \pi \cdot Area / (Perimeter)^2$	
Roundness	$R = 4 \cdot Area / (\pi l_m^2)$	$l_m$ : maximum axis length of the particle
	$R = 4 \cdot \pi Area / (r^2)$	$r$ : radius of the circumscribed circle
Compactness	$C = 4 \cdot \pi \cdot Area / (Convex Perimeter)^2$	
Aspect ratio	$A_{ratio} = Length / Diameter circular$	
	$A_{ratio} = Length of longest feret / Length of shortest feret$	
Average area		
Fraction pearlite		measured after 4% Nital etching



## Methodology for Skin Quality Measurement of Ductile Iron Castings

In previous AFS sponsored research the influence of a number of process variables on the tensile properties and surface roughness of thin-wall ductile iron (TWDI) castings was investigated. The test casting (Fig. 6) was a 3-plates vertical casting with plates of thickness 6, 2.5 and 3.5 mm, poured in alkyd-urethane resin-bonded molds (see ref. 10 for details of melting and casting). Extensive statistical analysis was conducted to evaluate the experimental results on 32 test-plates. The complete results have been reported in an AFS paper<sup>10</sup>.

For this research samples from heat 50602 (chemical composition 3.67%C, 2.92%Si, 0.04%Mg), mold no. 8 (pouring temperature 1366°C) (2491°F) and mold 4 (pouring temperature 1400°C) (2566°F) were analyzed. The test-plates were cross sectioned and metallographic samples were prepared. On each metallographic sample a region of 1 mm depth from the sample surface was used in the analysis, as shown in Fig. 7.

The microstructural features were evaluated using the Clemex Vision version 3.0 image analysis software and are summarized in Table 2. For additional details on these quantities the reader is referred to reference <sup>11</sup>.

An image analysis routine was created to conduct graphite shape and pearlite content measurements. In the routine, a 0.4x0.1mm frame at a magnification of 200X was created as a boundary for the measurements. The gray threshold was adjusted for the appropriate graphite or pearlite

measurement. For the pearlite measurement, the threshold was adjusted to remove the graphite nodules from the measurement. Next in the routine, the total area and average area were measured, followed by the object measurements of sphericity, roundness, aspect ratio, and compactness.

This routine was performed on a number of consecutive frames sufficient to cover the depth of the casting skin. Data was collected for each of the ten frames then an average value for each frame was calculated. Microhardness measurements were taken on the 6mm sample from molds 6, 8, and 4 every 0.1mm. Measurements were made using a number of consecutive frames based on the depth of the casting skin. The routines are presented in Fig. 8.

The tabulated experimental results for mold 8 are presented in Table 3. Additional data on other molds can be found in ref. <sup>12</sup>. The data in Table 3 were used to plot the variation of the average graphite shape parameters and the graphite area from the surface to the inside of the sample. An example of the analysis can be seen by examining Fig. 9. It is seen that all shape parameters increase rapidly until a certain subsurface depth (0.15-0.25mm), after which the numbers remain relatively constant (Fig. 9 left). The same is true for the graphite area (Fig. 9 right) where the values pick at 0.25mm. Clearly, the average area is a more reliable indicator of skin depth than graphite shape factors.

Fig. 10 is a representative image of the unetched as-cast surface of a 3.5mm sample. These data imply that the thickness of the casting skin in these samples is about 0.15 to 0.25mm, and is not significantly influenced by the thickness of the plate.

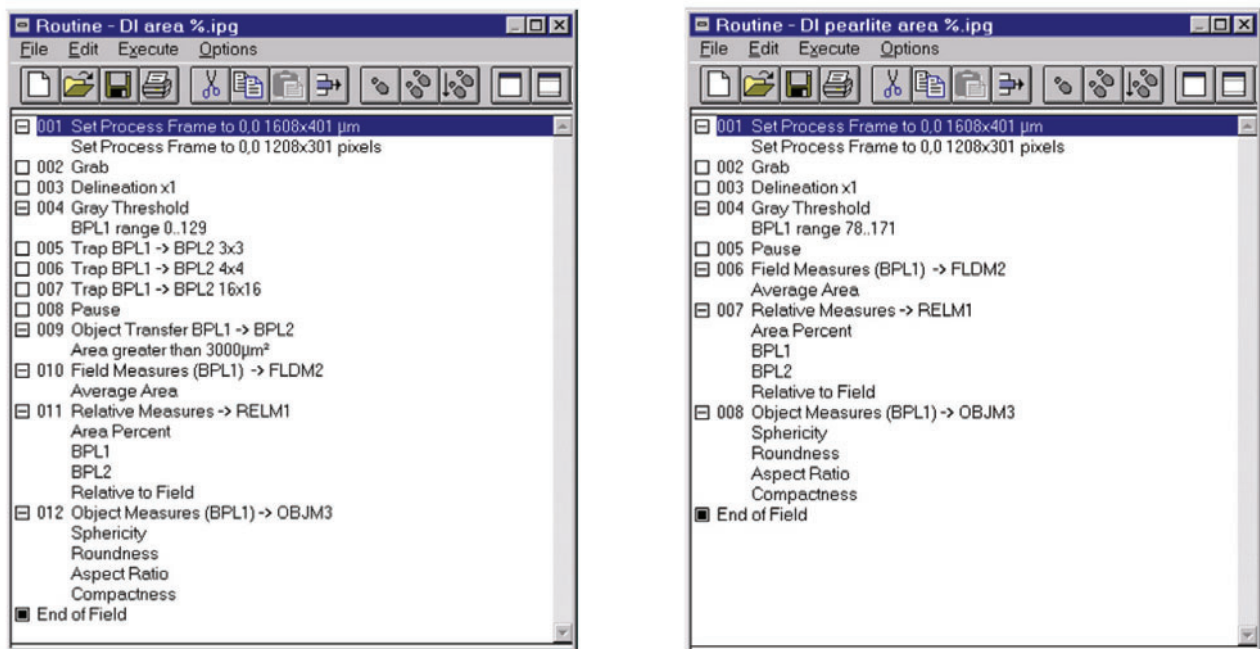


Figure 8. Image analysis routines for measuring graphite shape (left) and percent pearlite (right).

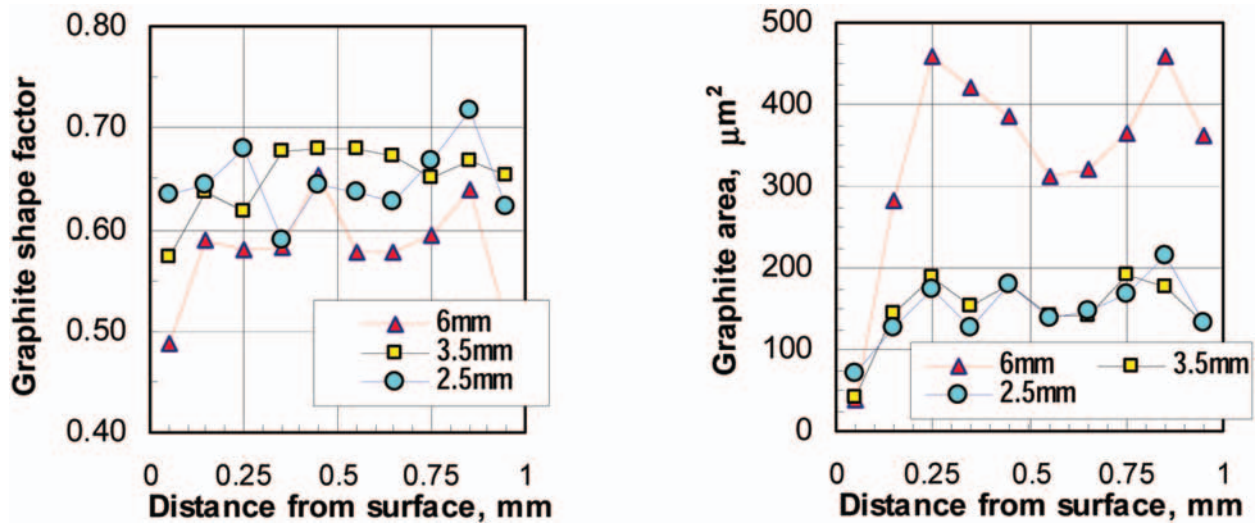


Figure 9. Graphite shape (left) and graphite area (left) variation from the surface inward for plates from mold 8.

Table 3 Average values for the graphite shape and area, mold 8.

Field	Distance (mm)	Sphericity	Roundness	Compactness	Average shape factor	Avg. Area ( $\mu\text{m}^2$ )
<b>2.5mm thick plates</b>						
1	0.05	0.55	0.60	0.74	0.63	71.85
2	0.15	0.60	0.58	0.75	0.64	126.34
3	0.25	0.61	0.64	0.79	0.68	174.77
4	0.35	0.53	0.53	0.71	0.59	127.62
5	0.45	0.55	0.60	0.78	0.64	180.47
6	0.55	0.57	0.58	0.76	0.64	137.47
7	0.65	0.55	0.57	0.76	0.63	148.38
8	0.75	0.59	0.63	0.78	0.67	167.53
9	0.85	0.62	0.69	0.84	0.72	214.14
10	0.95	0.55	0.57	0.75	0.62	131.00
<b>3.5mm thick plates</b>						
1	0.05	0.51	0.51	0.70	0.57	42.54
2	0.15	0.56	0.59	0.76	0.64	144.59
3	0.25	0.53	0.58	0.74	0.62	189.67
4	0.35	0.61	0.63	0.79	0.68	152.96
5	0.45	0.63	0.62	0.79	0.68	180.44
6	0.55	0.66	0.60	0.78	0.68	141.50
7	0.65	0.59	0.64	0.79	0.67	142.00
8	0.75	0.57	0.60	0.78	0.65	189.85
9	0.85	0.59	0.62	0.79	0.67	176.52
10	0.95	0.58	0.60	0.78	0.65	131.61
<b>6mm thick plates</b>						
1	0.05	0.49	0.40	0.57	0.49	37.33
2	0.15	0.50	0.55	0.72	0.59	283.18
3	0.25	0.51	0.53	0.70	0.58	459.23
4	0.35	0.47	0.55	0.73	0.58	419.36
5	0.45	0.50	0.65	0.81	0.65	384.72
6	0.55	0.46	0.56	0.71	0.58	311.38
7	0.65	0.47	0.54	0.72	0.58	320.86
8	0.75	0.50	0.55	0.73	0.59	364.59
9	0.85	0.49	0.64	0.79	0.64	459.04
10	0.95	0.43	0.45	0.65	0.51	360.49

The percent pearlite for the 6mm sample was measured versus the distance from the as-cast surface (Fig. 11). There is a significant decrease in the amount of pearlite from the as-cast surface to 0.25mm into the sample. The Vickers microhardness measurements versus the distance from the as-cast surface are superimposed on the same graph. The hardness decreases with distance into the sample, confirming the decrease in the fraction pearlite from the surface inward. Fig. 12 is a representative image of the pearlite found near the as-cast surface on the 6mm sample and the microhardness imprints.

Flake graphite in the skin was only present on mold 4 heat 50602 (other details in ref. 10). Fig. 13. shows the Vickers microhardness measurements versus the distance from the

as-cast surface. The hardness decreases with distance from the surface. Fig. 14 shows the flake graphite found near the as-cast surface. Only the 2.5 and 6mm samples of mold 4 contained flake graphite.

Based on these data it was concluded that the graphite shape parameters (sphericity, compactness and roundness) combined with graphite area measurements provide reliable information for the evaluation of graphite degradation in the casting skin. Microhardness measurements are useful when a pearlitic rim occurs. Based on graphite shape degradation, graphite depletion and microhardness measurements, the average thickness of the casting skin for the thin DI plates investigated ranges from 0.15 to 0.25mm.

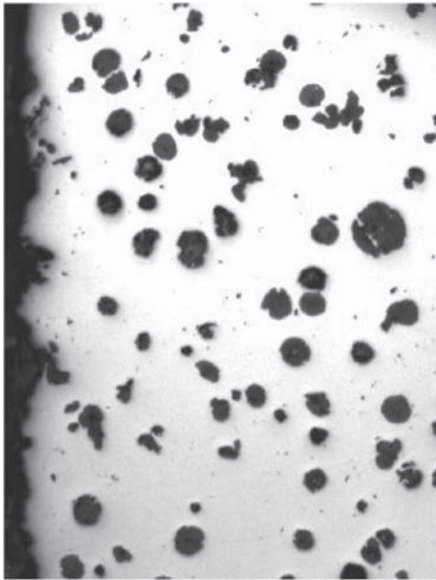


Figure 10. Unetched microstructure next to the casting surface for a 3.5mm sample, mold 8. Note graphite depletion in the skin. Magnification 200X.

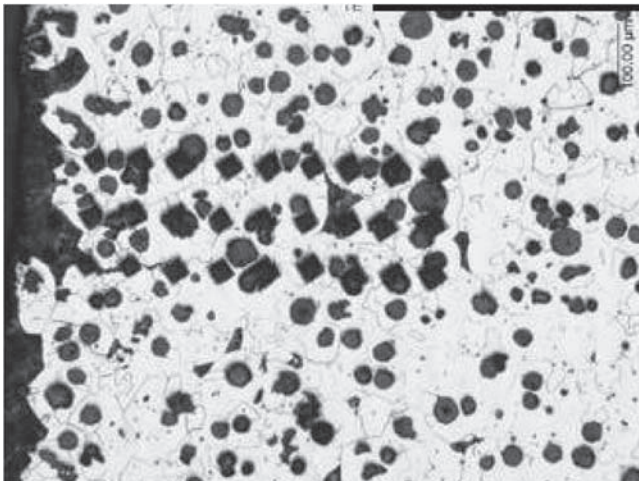


Figure 12. Pearlite near the as-cast surface of the 6mm plate from mold 8 and microhardness imprints.

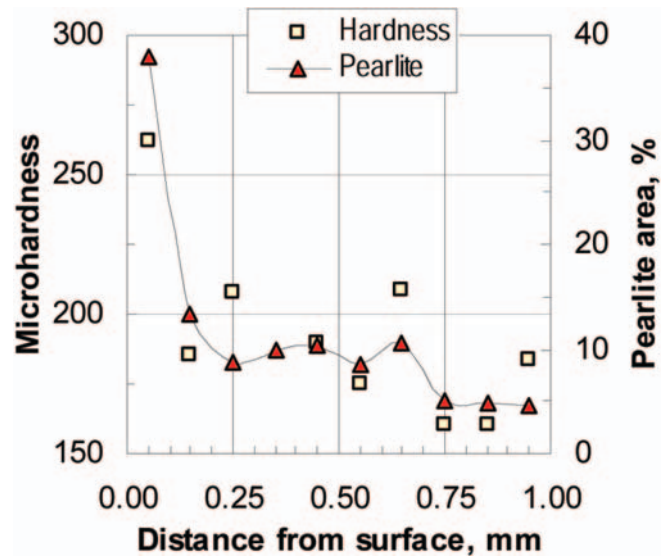


Figure 11. Microhardness and pearlite area of the 6mm plate from mold 8.

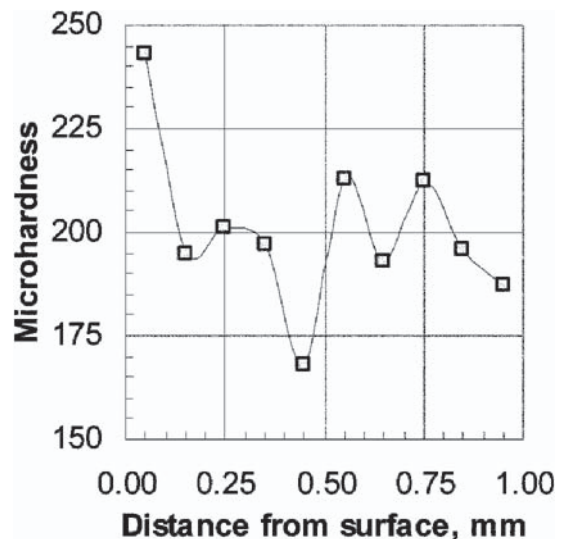
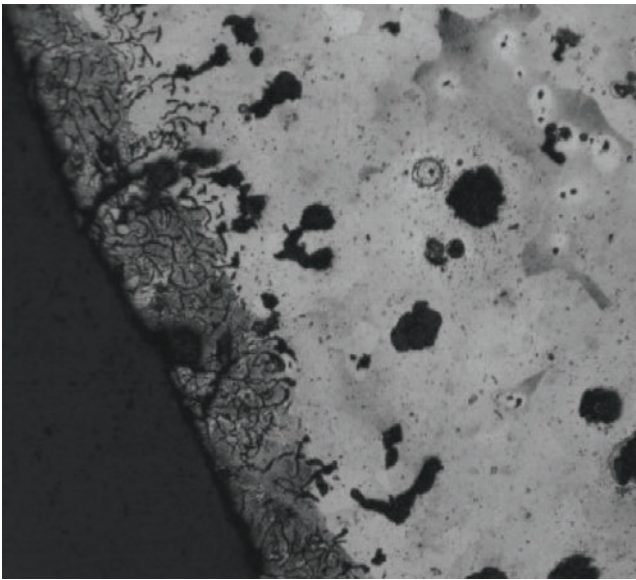


Figure 13. Microhardness measurements on the 6mm plate from mold 4.





**Figure 14. Flake graphite at the as-cast surface of a plate in mold 4. Magnification 500X.**

### Methodology for Skin Quality Measurement of Compacted Graphite Iron Castings

L-shaped sections of cylindrical test CG iron castings (Fig. 15) were received from Ashland Casting Solutions<sup>7</sup> for metallographic evaluation and microhardness measurements along the skin surface. Fig. 16 shows a schematic of the mold and a test casting assembly. It is a bottom gated three-part mold of an 8" cylinder diameter, which accommodates four 2"x2" cylindrical cores, and features a center located 8" riser. The molds were made with silica sand, GFN 55-60 and a phenolic urethane no-bake binder. The cores were made with zircon sand, GFN 108-112 and a cold-box binder at typical addition levels. While three samples were analyzed only results for one sample will be presented here, as the others were similar. Microstructural and microhardness investigation was conducted from the sample surface inward at four positions marked 0", 0.5", 1", and 1.5".

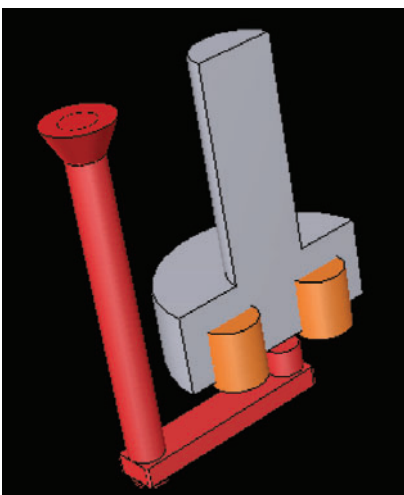


**Figure 15. Sectioned casting, cores and gating system (Ashland design).**

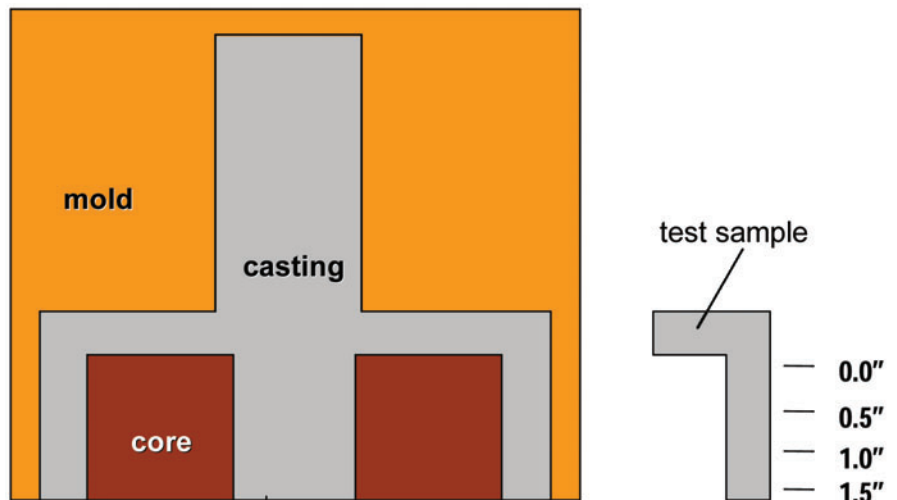


**Figure 16. Schematic of the mold and test sample. The numbers on the right are the metallostatic height.**

Quantitative analysis was conducted as described in section 4.1. The routine was performed on several consecutive frames beginning at the as-cast surface. Data was collected for each frame and then an average value for each frame was calculated. For shape measurements at positions 0" and 0.5", the routine was performed on 10 consecutive frames. For positions 1" and 1.5", the measurements were made on 15 and 25 consecutive frames, respectively.

Microhardness measurements were performed every 0.1mm from the surface of the sample. For each position three imprints were measured. The recorded data is the average of these three measurements.

Fig. 17 shows a montage at each position of the etched as-cast surface of the CG iron sample taken at 100X magnification. The following characteristic microstructural regions can be identified: flake graphite near the surface; next, fine flake and compacted to coarse compacted; coarse compacted and some spheroidal and exploded graphite further away from the surface. Position 1.5" has the largest amount of flake graphite while position 0" has the smallest amount. The amount of pearlite varies between positions. Position 1.5" has the smallest amount of pearlite while position 0" has the largest amount.

The measured data were used to plot the variation of the graphite shape parameters from the surface to the inside of the sample, for the 0", 0.5", 1", and 1.5" positions. The graphs for the 0" and 1.5" positions are presented in Fig. 18, left column. The aspect ratio data are plotted in Fig. 18, right column.

From the plots in Fig. 18 it is possible to attempt to evaluate the thickness of the skin. All shape factors increase in value as the distance from the surface increases, reach a maximum and then stabilize more or less, although some significant variation may occur after the first maximum. The aspect ratio evolves in an opposite manner.



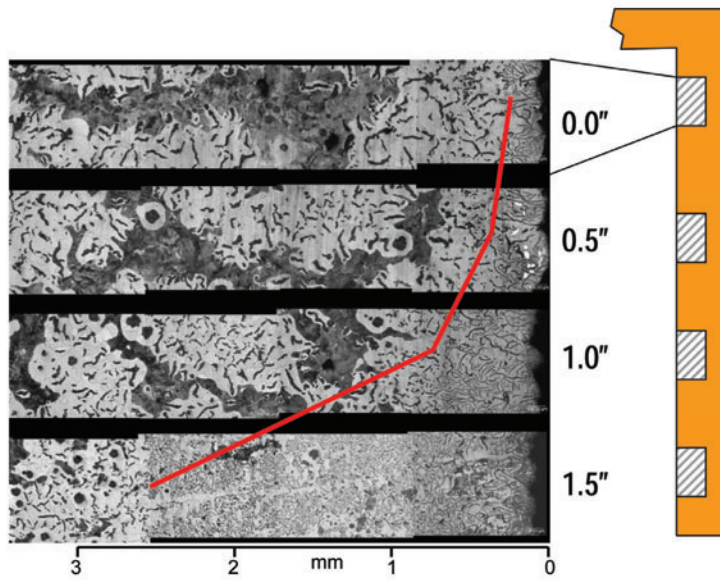
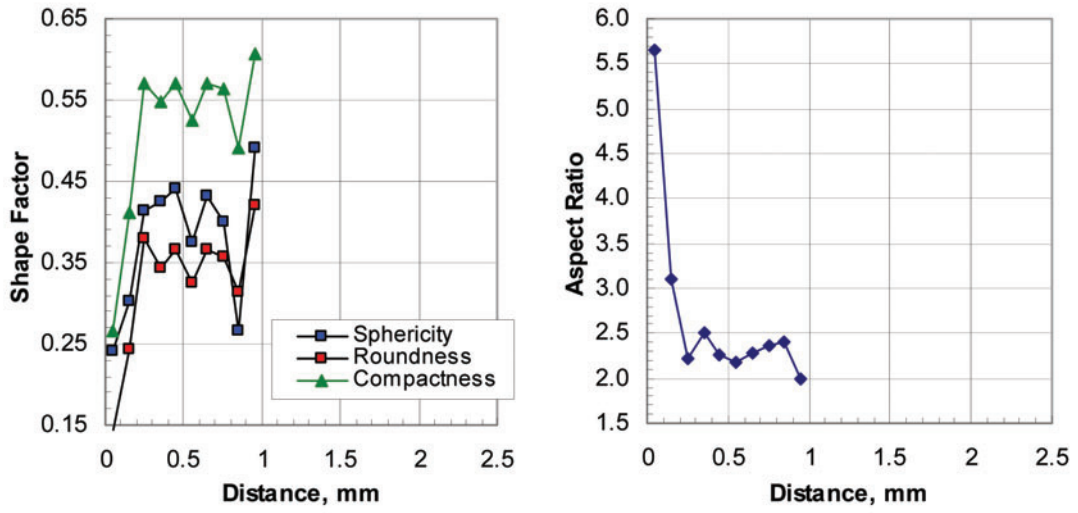
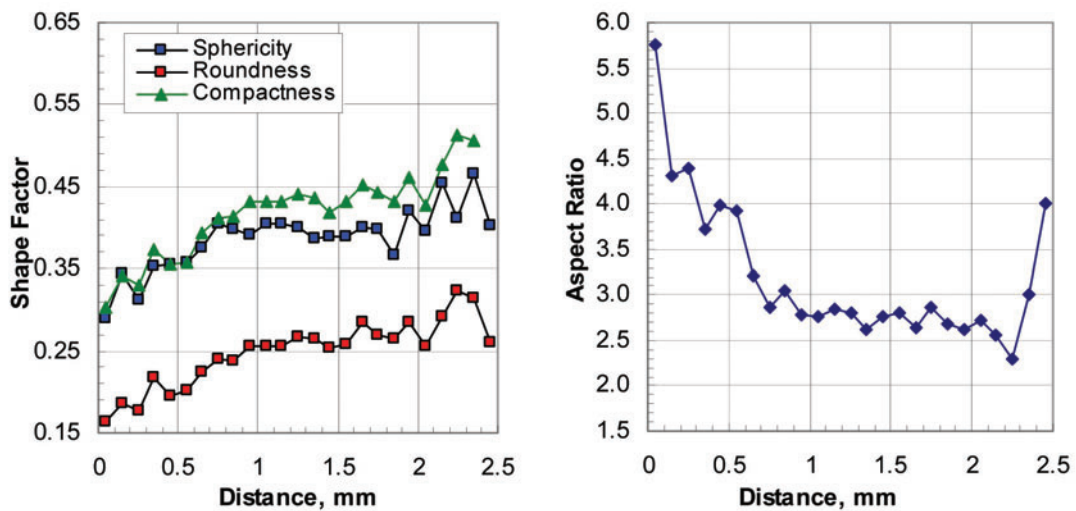


Figure 17. Microstructure of casting skin in the CGI test casting in Figure 15 as a function of relative metallostatic height.



a) Position 0"



b) Position 1.5"

Figure 18. Graphite shape variation with distance from surface for the 0" and 1.5" positions on the CGI sample.

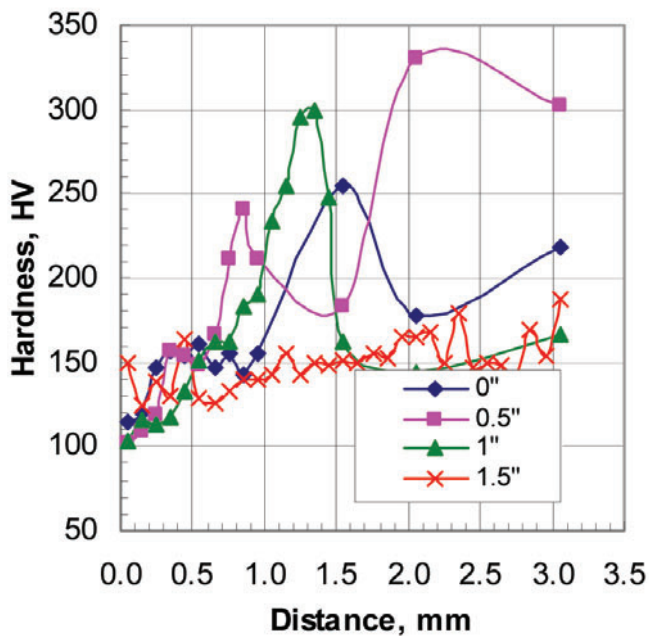


Figure 19. Microhardness measurements at each position on the CGI iron sample.

Fig. 19 shows the Vickers microhardness measurements versus the distance from the as-cast surface. Significant increase in hardness is seen at depths of 0.85mm and 1.25mm for positions 0.5" and 1", respectively. This increase corresponds to the regions of pearlite found at these positions. For position 0" the pearlite hardness is only reached at a depth of 1.55mm.

The experimental data that correlate the thickness of the casting skin with the position (height) in the casting are summarized in Fig. 20. The thickness of the casting skin ranges from 0.7 to 2.5mm for the CGI investigated.

From the work on CGI presented here it is apparent that while microhardness may give an indication on the extent of the casting skin, it is not very reliable because of the discontinuities in the pearlite field and the influence of the graphite. It is still a useful indication when used in conjunction with the image analysis of graphite shape. The use of the average of the three parameters may also be interesting. Aspect ratio also gives useful information for CGI, while it does not seem to work for DI.

## Skin Quality Quantification

### Experimental Approach

While the methodology for skin quality measurement was developed for both DI and CGI, the quantification of the skin effect on mechanical properties involved only thin

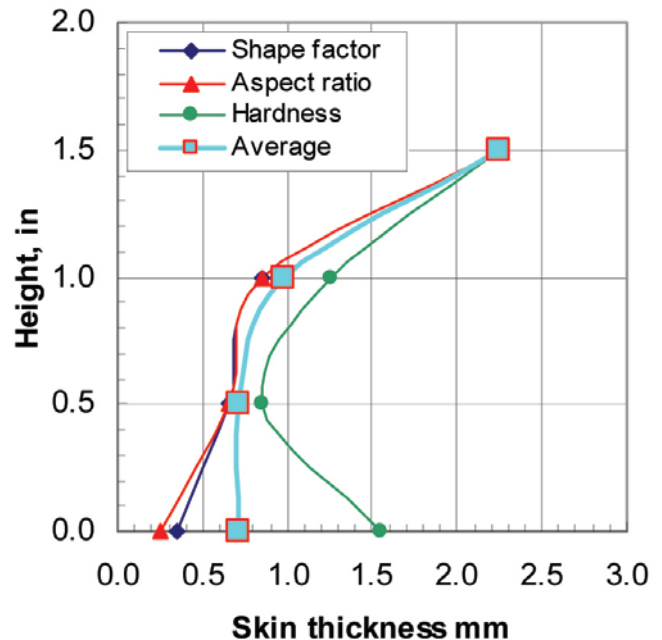


Figure 20. The influence of the position in the casting (metallostatic height) on the thickness of the casting skin evaluated through three different parameters.

wall DI castings. A test casting was designed using the cad software Ironcad and the simulation software Magmasoft. The design objectives included: test casting large enough so that samples for tensile testing can be machined; mechanical testing to be performed on as-cast and machined samples; the characteristic cooling rate of the test sample should be about 10K/s; quiescent filling of the mold.

After a large number of computer experiments<sup>12</sup>, the pattern shown in Fig. 21 was adopted. The pattern consisted of three plates of length 100mm, width 27mm, and thickness of 2.5, 4.0 and 6.0mm, respectively and an added filter.

Three stacked molds (one sodium silicate sand and two resin bonded sand) including five horizontal test castings (plates) each were produced (Fig. 22). The three molds were tilted 15 degrees for pouring. A 10 ppi filter was used in each mold. In addition to these molds buttons for metallographic analysis as well as chilled disks for chemical analysis were produced.

A 100lb melt was produced in the 300lb induction furnace at Ashland Inc. The charge composition is listed in Table 4. After melt down and correction the molten metal was transferred into a ladle and modified in stream with 1.73% FeSi50Mg5 alloy. After the completion of the Mg reaction, the slag was removed and 0.075% FeSi75 was added on top of the metal and then mixed as post inoculant. The molds and the buttons were poured at a temperature of 1350°C. The castings were sand blasted.

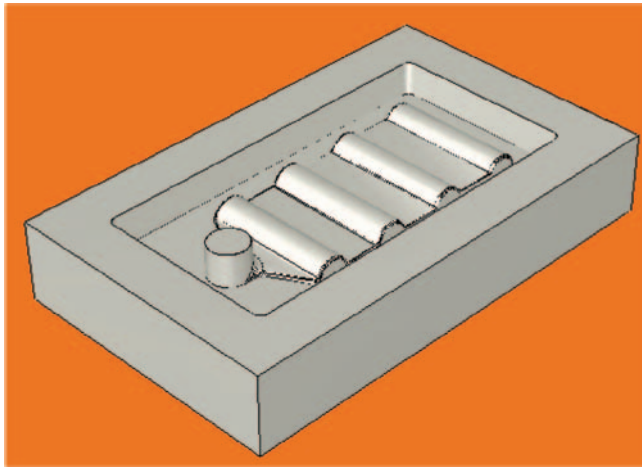


Figure 21. Pattern used for mold production.

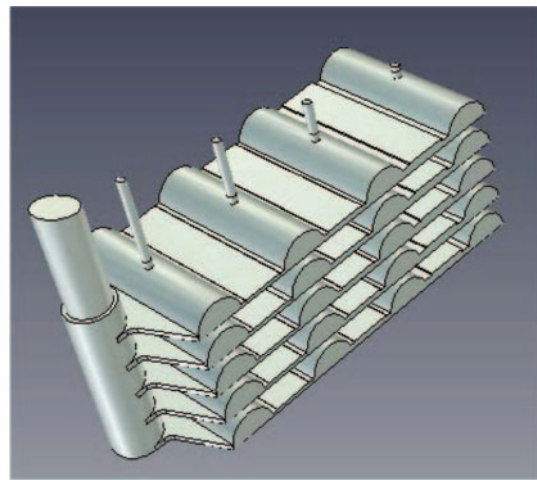


Figure 22. Stacked and tilted casting.

Table 4. Charge composition and chemical analysis of materials used.

Material	Chemical composition, %						Addition
	C	Si	Mn	P	S	Mg	%
Sorel pig iron	4.25	0.05	0.028	0.044	0.016	-	55
Steel scrap	0.2	0.5	0.2	0.03	0.02	-	5
CGI returns	3.47	2.23	0.15	0.033	0.016	-	40
FeSi50Mg5	NA	50	NA	NA	NA	5	1.73
FeSi75	NA	75	NA	NA	NA	NA	1.0

Table 5. Chemical analysis.

Material	Chemical composition, %					
	C	Si	Mn	P	S	Mg
Base heat	3.76	1.80	0.080	0.054	0.012	-
Treated ductile iron	NA	2.73	0.082	0.061	0.039	0.039

## Experimental Results

Spectral chemical analysis was performed on chilled coins by Liberty Casting. The chemical analyses of the base metal and of the metal after Mg treatment and post-inoculation are given in Table 5.

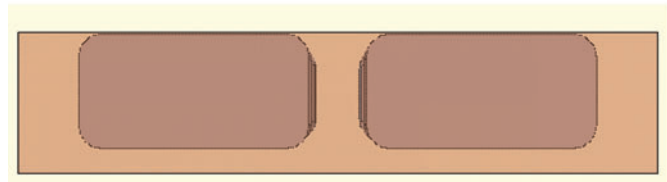
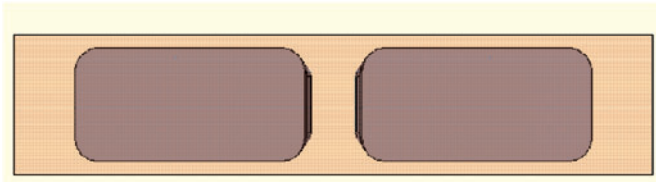
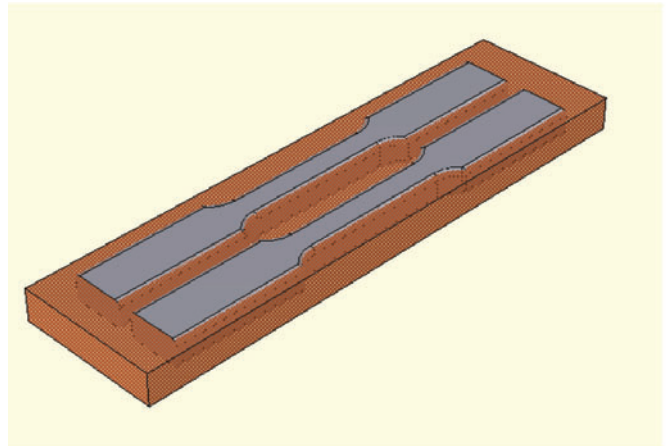
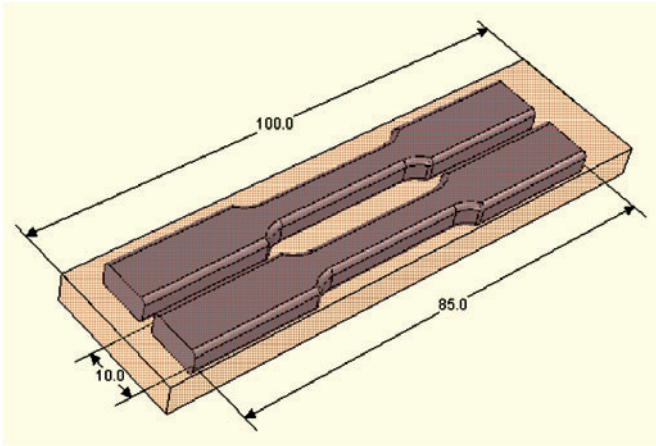
Many attempts were made at measuring the surface roughness of the bottom side of the samples but, because the surface was obtained by scraping the corebox, the roughness was larger than the measurable limits of the instrument. To control the surface roughness variable the bottom side of all samples was machined to a smooth finish using a water-jet process.

From each plate, two flat ASTM test samples for mechanical testing were machined as shown in Fig. 23. The dimensions of the test samples are given in Fig. 24.

The thickness of the casting skin was evaluated on the basis of graphite shape change as described in section 4. The complete tabulated measured data can be found in ref. 12.

Some examples of casting skin microstructure are presented in Fig. 25 and Fig. 26. Note the graphite depletion on the skin of the samples (Fig. 25) and the pearlitic rim on the etched samples (Fig. 26).





fully machined (M)

machined only on bottom side (AC on top side)

Figure 23. Fully machined and partially machined (top surface as cast) samples.

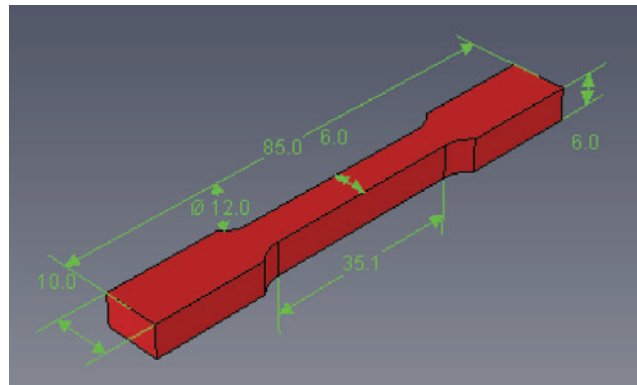


Figure 24. Machined ASTM test sample.

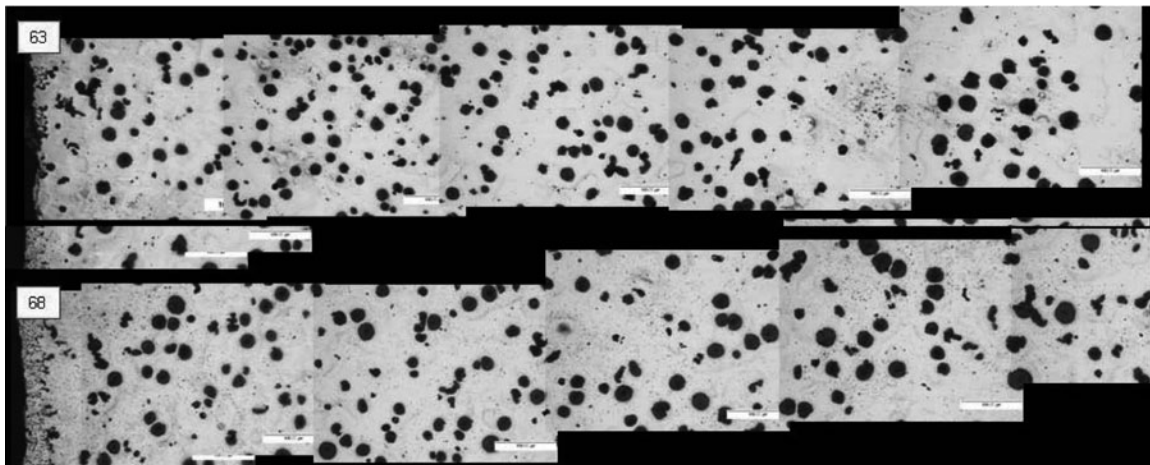


Figure 25. Graphite morphology for samples #1ACp1/6mm (63) and p2/6mm (68) - unetched.

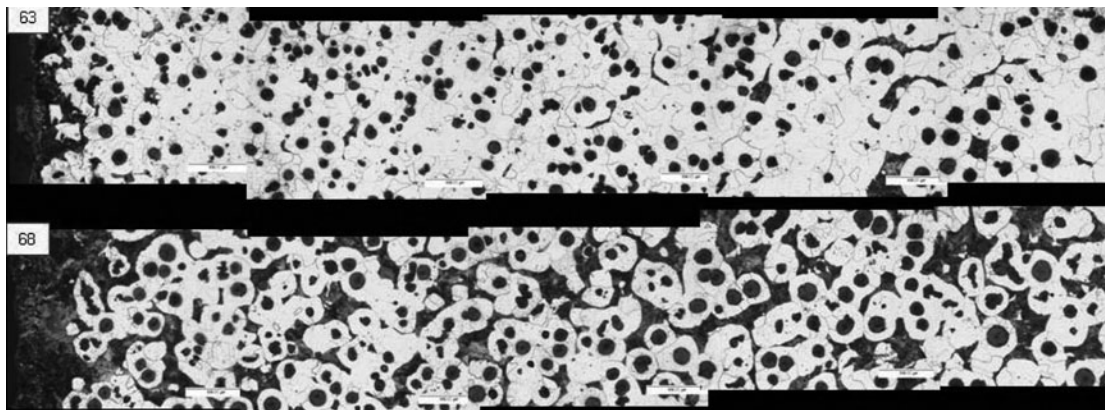


Figure 26. Microstructure of samples #1ACp1/6mm (63) and p2/6mm (68) - etched.

Table 6. Experimental measurements.

Mold	Surface	Plate	Thick-ness (mm)	Metal-lost static height, mm	Skin depth (mm)	Rough-ness (Top) ( $\mu\text{m}$ )	UTS (ksi)	Yield Str. (ksi)	Elong. at fract. (%)
#1 sodium silicate	M	p1	4	33.4		11.27	64.5	41.6	13.8
	AC		6	66.9	0.25	15.93	53.9	37.2	7.3
	M	p2	4	59.7		21.56	65.4	42.8	10.0
	AC		6	93.2	0.15	15.80	71.5	57.4	5.2
	M	p3	2.5	71.5		15.33	63.9	45.5	11.0
	M		4	86.0		20.82	79.1	49.3	11.3
	M		6	119.5		25.14	78.8	48.4	10.9
	M	p4	2.5	97.8		22.39	66.1	44.2	21.7
	M		4	112.3		21.39	68.5	43.9	14.9
	M		6	145.8		22.55	67.8	43.6	17.4
#2 resin bonded	AC	p1	2.5	18.9	0.25	15.86	62.5	41.5	18.1
	AC		4	33.4	0.20	17.60	63.9	38.9	13.1
	AC		6	66.9	0.15	16.37	68.5	51.3	15.7
	AC	p2	2.5	45.2	0.23	19.91	60.8	39.2	13.2
	AC		4	59.7	0.35	22.69	62.4	39.0	18.2
	AC		6	93.2	0.27	26.27	62.2	40.8	16.7
	AC	p3	2.5	71.5	0.45	14.32	60.9	39.5	11.7
	AC		4	86.0	0.38	15.37	62.3	40.1	18.1
	AC		6	119.5	0.25	14.02	62.1	40.8	17.5
	AC	p4	2.5	97.8	0.28	18.02	63.9	42.0	17.0
	AC		4	112.3	0.35	19.84	63.1	42.8	16.4
	AC		6	145.8	0.35	22.18	67.3	43.4	18.9
	AC	p5	2.5	124.1	0.25	18.67	62.7	38.9	15.3
	AC		4	138.5	0.26	19.45	62.6	40.7	18.5
	AC		6	172.1	0.35	23.43	67.0	43.3	17.4
#3 resin bonded	M	p1	2.5	18.9	NM	21.28	69.9	45.8	10.8
	M		4	33.4	NM	19.68	62.8	36.4	17.1
	M		6	66.9	NM	24.40	63.7	42.5	20.2
	M	p2	2.5	45.2	NM	25.93	65.0	43.9	15.3
	M		4	59.7	NM	18.75	67.7	45.6	10.4
	M		6	93.2	NM	19.32	77.3	47.5	11.2
	M	p3	2.5	71.5	NM	23.46	63.0	41.6	14.9
	M		4	86.0	NM	19.26	65.9	45.0	14.0
	M		6	119.5	NM	22.11	75.4	49.2	7.1
	M	p4	2.5	97.8	NM	17.62	62.1	41.9	10.2
	M		4	112.3	NM	19.28	67.4	45.2	13.3
	M		6	145.8	NM	21.15	76.3	50.9	13.1
	M	p5	2.5	124.1	NM	25.41	62.6	44.2	14.5
	M		4	138.5	NM	23.60	63.7	43.2	17.0
	M		6	172.1	NM	29.38	66.1	44.5	15.7

The complete characterization data are presented in ref. 12. The pouring order is indicated by the # listed in front of the molding aggregate. The surface of the test samples was either as cast -AC (only the upper surface), or machined -M. The metallostatic height varies for each plate (test casting) because the molds were poured tilted 15 deg. with respect to the horizontal. It also increases from plate 1 to plate 4 because of the mold stacking. The roughness was measured only on the top surface. The bottom surface was too rough, as the mold surface was created by shaving the excess sand on top of the core box. The roughness was measured by the method described in reference 3 and reported as roughness average,  $R_a$ . All results for skin depth, roughness and mechanical properties are the average of two measurements.

## Discussion

### Variables Affecting the Casting Skin

Correlation analysis was conducted on the as-cast samples for which the skin thickness was measured. The results are given in Table 7. It is seen that the casting skin increases in thickness as the plates become thinner (the correlation coefficient is -0.24). However, there is considerable scatter of data (Fig. 27). To explain this behavior an understanding

of the mechanism of skin formation is required. This will be discussed in a later section.

The roughness increased with the metallostatic height (0.35). The correlation coefficient increased to 0.4 when all measured castings were included in the analysis (Fig. 28). This trend is reasonable, as mechanical penetration increases with metallostatic height.

### Variables Affecting the Tensile Properties

Correlation analysis was conducted only on the as-cast samples from mold #2, because the mechanical properties test samples had only one as-cast surface, while the samples from mold #1 had two as-cast surfaces. The results presented in Table 8 indicate that the tensile properties are favorably affected by increased plate thickness (see blue line on Fig. 29) and metallostatic height, but negatively affected by thicker casting skin (Fig. 30). The increase of tensile properties with plate thickness is explained by the thinner skin associated with the thicker plates.

The effect of roughness is inconclusive. This is not surprising. Indeed, as shown in Fig. 5, a significant increase in strength occurs only at roughness below  $10\mu\text{m}$ . For the analyzed samples the average roughness was considerably higher -  $18.6\mu\text{m}$ .

Table 7. Correlation analysis for all as-cast samples.

<i>As cast</i>	<i>Skin depth</i>	<i>Roughness</i>
Plate thickness	-0.24	0.20
Metall. Height	0.28	0.35

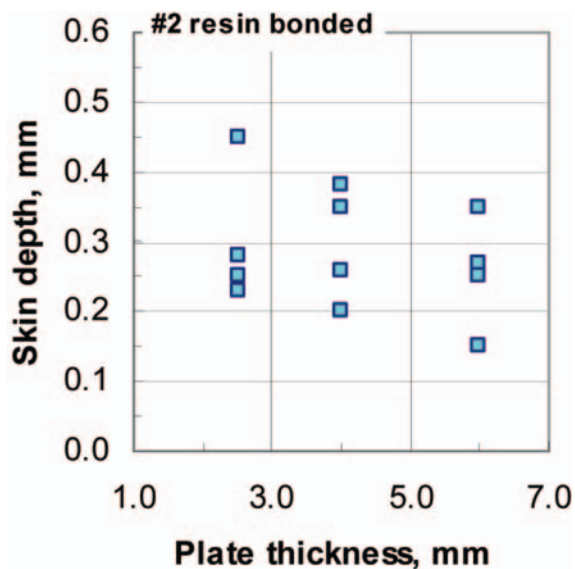


Figure 27. Variation of the thickness of the skin depth with the thickness of the test plates.

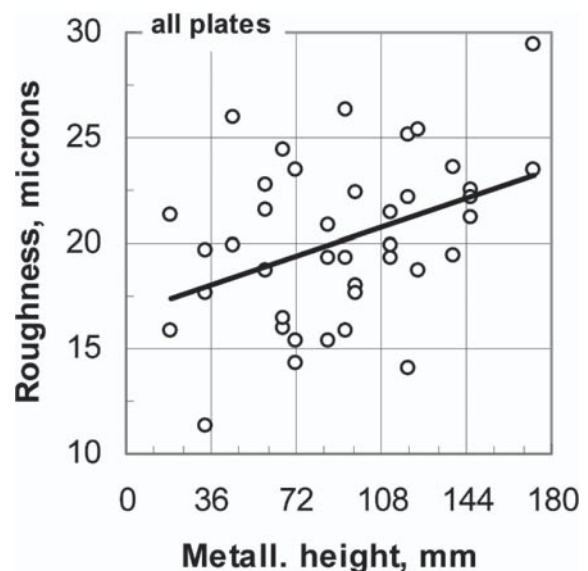
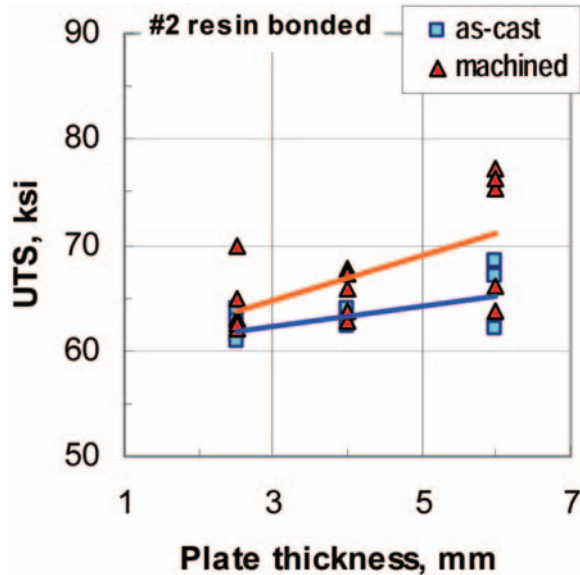


Figure 28. Variation of measured roughness on the top surface of the plates with the metallostatic height.



**Table 8. Correlation analysis for as-cast samples (mold #2).**

<i>As cast</i>	<i>UTS</i>	<i>Yield Str.</i>	<i>Elong.</i>	<i>Skin depth</i>	<i>Roughness</i>	<i>Thickness</i>
Yield Str.	0.80	1.00				
Elong.	0.29	0.19	1.00			
Skin depth	-0.23	-0.33	0.07	1.00		
Roughness	0.21	-0.03	0.28	0.07	1.00	
Thickness	0.61	0.52	0.40	-0.11	0.37	1.00
Metall. Height	0.37	0.15	0.43	0.30	0.35	0.47



**Figure 29. Variation of tensile strength with the plate thickness.**

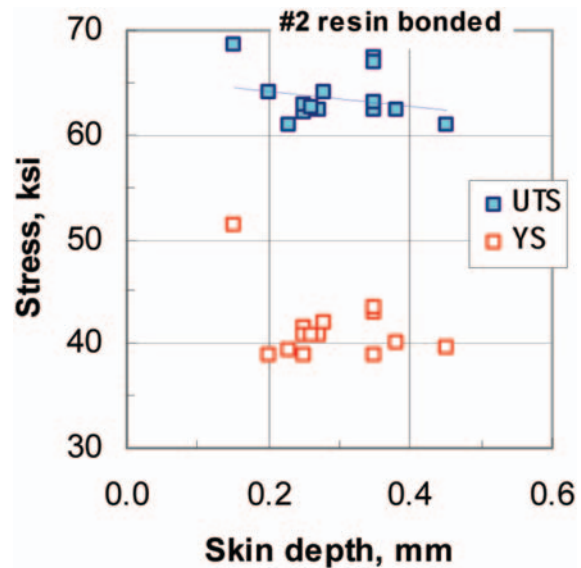


**Figure 30. Variation of tensile stress with the skin depth.**

**Table 9. Correlation analysis for machined samples.**

<i>Machined</i>	<i>UTS</i>	<i>Yield Str.</i>	<i>Elong.</i>	<i>Thickness</i>
Yield Str.	0.83	1.00		
Elongation	-0.46	-0.49	1.00	
Thickness	0.55	0.38	-0.04	1.00
Metall. Height	0.25	0.40	0.11	0.49

Results of correlation analysis on the machined samples are presented in Table 9. The trend of an increasing strength with plate thickness (Fig. 29) and metallosatic height is confirmed. The positive correlation between strength and metallosatic height may be the results of either i) higher material compactness with higher metallosatic pressure, or ii) higher plate thickness with higher metallosatic pressure resulting from the experimental setup (the plates within a casting follow the sequence 2.5, 4 and

6mm, with the 6mm being always higher than the other because of the tilting of the mold during pouring). Note that, unfortunately, for both as cast and machined samples metallosatic height correlates well with plate thickness ( $\geq 0.5$ ).

As expected the elongation decreases as strength increases (-0.46 for UTS and -0.49 for YS). This effect is less clear for as-cast samples (Fig. 32).

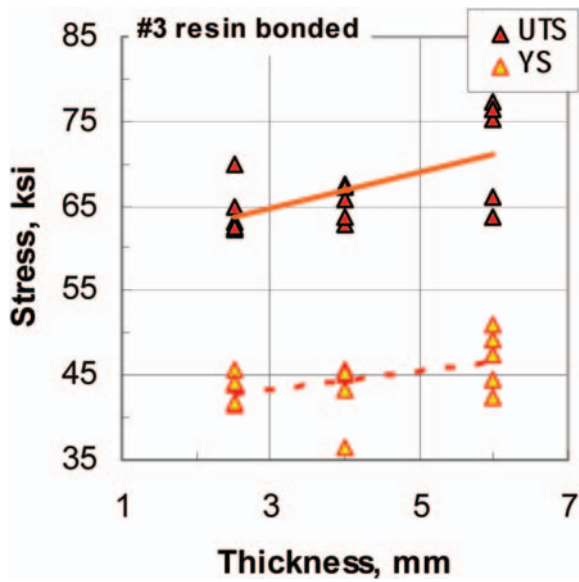


Figure 31. Variation of tensile strength with the plate thickness on fully machined samples.

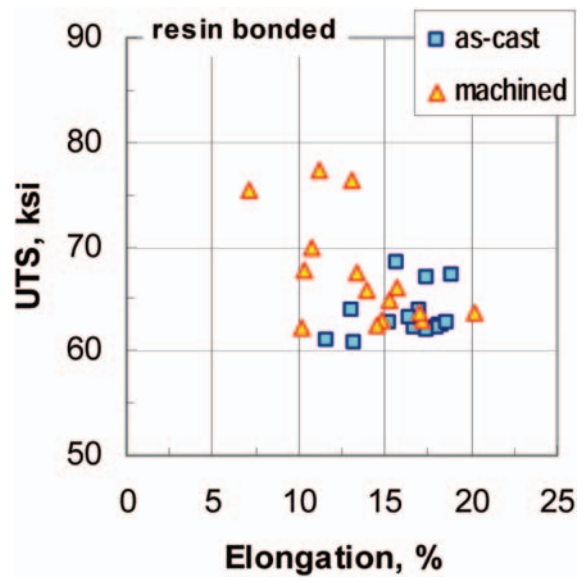


Figure 32. Correlation between tensile strength and elongation.

Table 10. Average mechanical properties on as-cast and machined samples.

Quantity	As-cast		Machined	
	Average	Range	Average	Range
UTS (ksi)	63.5	60.8-68.5	67.9	62.1-79.1
YS (ksi)	41.5	37.2-43.3	44.6	36.4-50.9

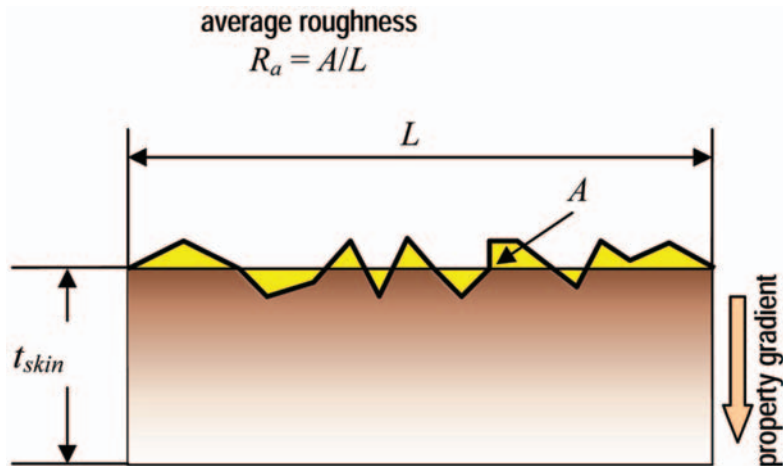


Figure 33. Characterization of skin quality.

Table 11. Regression analysis for as-cast samples (mold #2 only)

Quantity	Intercept	$t_{skin}$ (mm)	$R_a$	Std. error	Observations
UTS (ksi)	62.85	-7.19	0.14	2.36	15
YS (ksi)	45.45	-13.09	-0.008	3.21	15

## Calculation of Skin Quality

A skin quality factor for tensile strength is defined as the ratio between the as-cast ( $TS_{ac}$ ) and machined ( $TS_m$ ) tensile strength:

$$SF_{TS} = TS_{ac}/TS_m \quad (1)$$

From the data in Table 6, the average values in Table 10 are obtained.

Using Eq. (2) the average TS skin factor for these data is calculated as:  $SF_{TS} = TS_{ac}/TS_m = 63.5/67.9 = 0.93$ . Note that the same value is obtained for the yield strength skin factor.

To predict the skin factor, further quantification/calculation of skin quality must be performed using elements of characterization as shown in Fig. 33. They include: average roughness,  $R_a$ ; skin thickness,  $t_{skin}$ ; property gradient – describes the change of a certain quantity (e.g., nodularity, % pearlite, microhardness) over the thickness of the skin. The tensile specimens machined from plates of different thickness are tested in as cast condition. Linear regression analysis is then conducted to correlate  $TS$  to the various skin features. An equation having the following shape is produced:

$$TS_{ac} = a + b \cdot R_a + c \cdot t_{skin} + d \cdot dN/dx + \dots \quad (2)$$

where a, b, c, d are coefficients to be determined from the regression analysis of the experiments,  $dN/dx$  is the nodularity gradient and others are as defined in Fig. 33.

Regression analysis data for tensile and yield strength are presented in Table 11. With these equations the skin factor of any sample can be calculated from metallographic analysis only. Because only one as-cast surface was used in these experiments, the  $R^2$  was very poor. Consequently these regression equations should only be considered an example.

## Conclusions

The range of skin depth for the TWDI plates investigated is between 0.15 and 0.45mm. It was found that the skin depth decreases with increased test plate thickness.

The roughness increased with higher metallographic pressure. Within the range of roughness investigated in this research (average  $R_a = 18.6\mu\text{m}$ ) there was no clear trend on the tensile properties, other than the machined samples exhibiting higher properties than the as-cast ones.

The strength decreased with thicker casting skin and increased with thicker test plates. The tensile and yield strength skin factor was about 0.93. This should be viewed as an upper limit, as only one of the surfaces of the test plates was as-cast.

The results presented in this section are mostly semi quantitative because the “as-cast” test samples had in fact only one of four surfaces as-cast. A better test casting that will include more casting skin when tested “as-cast” should be designed.

## Mechanism of Casting Skin Formation

As evident from the various microstructures presented in this report, the three main metallographic characteristics of the skin casting of ductile and compacted graphite iron are graphite degradation, graphite depletion and pearlitic rim. We believe that these microstructural changes can be explained by liquid state and solid state diffusion mechanisms.

During the residency of molten metal in the mold and before solidification begins oxygen or sulfur from the mold diffuses in the adjacent liquid shell of the casting and reacts with Mg, Ce or other graphite modifiers in the melt. This will induce graphite degradation in the following sequence: 1) SG degenerates to CG; 2) CG degenerates to lamellar graphite; 3) type A - lamellar graphite degenerates to type D.

Alternatively, the same diffusion processes can result in complete depletion of graphite in DI. This depletes the skin of ferrite nuclei during the solid state transformation and may result in a pearlitic rim.

Other elements (e.g. C or S) can diffuse in liquid or solid state producing carbon-rich layers in the casting. During the solid state transformation these layers become the pearlite rim.

The plausibility of this theory will be checked through calculations.

## Graphite Degradation Rim

Let us start by examining some microstructures presented earlier in this report. From Fig. 17 it is noted that as the metallographic height increases from 0 to 1.5in., so does the skin thickness (red line on the figure). Let us first explore the graphite degradation rim. Graphite degeneration (degradation) can only occur because of:

- loss of Mg or Ce – possible causes are fading or chemical combination with S or O;
- poisoning by deleterious elements such as Te, Sb, As, etc.

In this case it is reasonable to assume that Mg from the melt was tied by oxygen or/and sulfur diffusing from the mold. A higher Mg level should result in thinner skin. Indeed, recent work<sup>6</sup> showed this to be true. Thus, the main cause of graphite degradation rim is Mg fading in the outer layer of the casting.



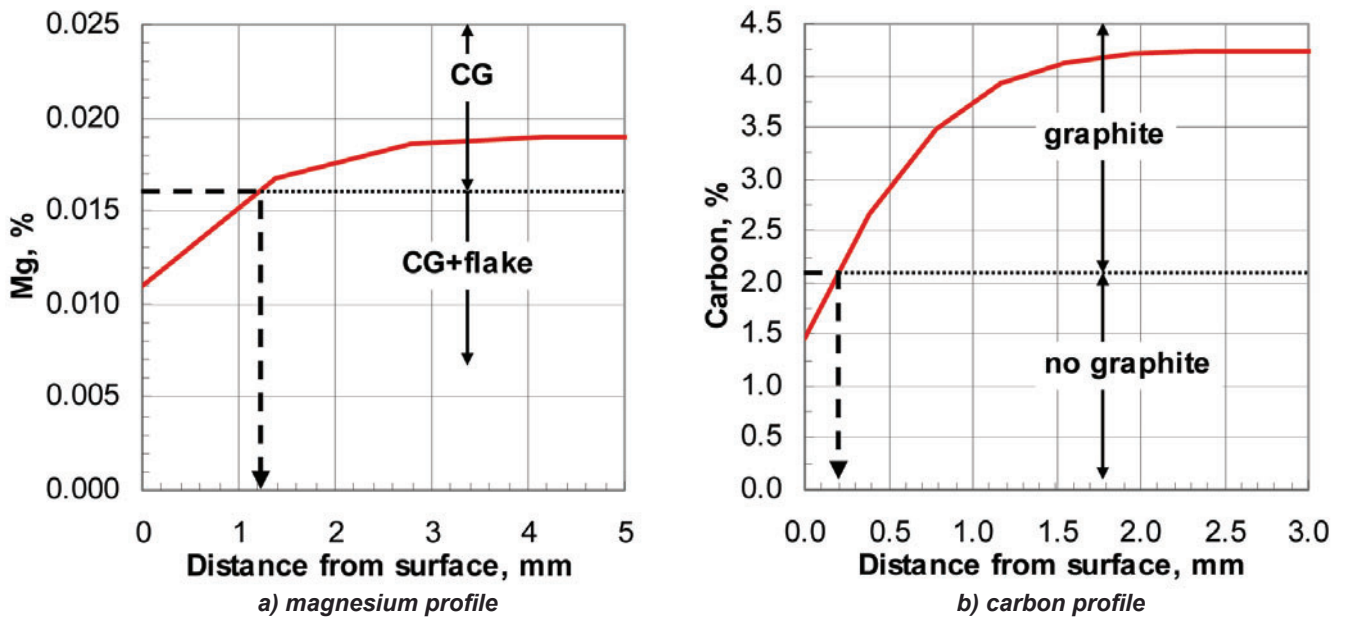


Figure 34. Magnesium and carbon content profile across the CGI test sample in Fig. 16.

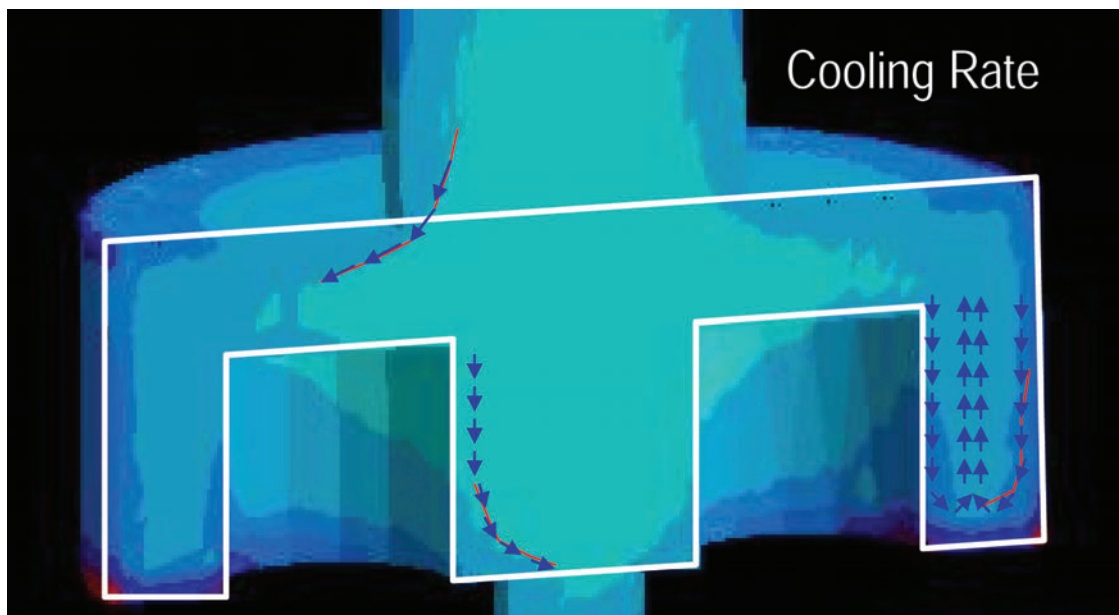


Figure 35. Magmasoft calculated cooling rate and flow in the CGI test casting.

To verify this hypothesis a Mg diffusion model was developed. The basic assumptions of the model included: 1) Mg sink at mold/metal interface (there is enough oxygen; oxygen – Mg reaction is instantaneous); 2) No liquid convection; 3) Initial Mg residual of 0.019%. The diffusivity of Mg in liquid iron was taken as  $2 \cdot 10^{-8} \text{ m}^2/\text{s}$ . The local solidification time calculated with the Magmasoft code for the test sample in Fig. 7 was 70s.

The governing equation is the solute diffusion equation:

$$D \frac{\partial^2 C}{\partial x^2} = \frac{\partial C}{\partial t} \quad (3)$$

where  $D$  is Mg diffusivity,  $C$  is composition,  $x$  is distance and  $t$  is time.

The results of the calculation are presented in Fig. 34a. Assuming the lower level of Mg required for CG formation to be 0.016%, the model predicts the thickness of the graphite degradation layer to be 1.2mm. The average measured graphite degradation rim is in the range of 0.7 to 2.6mm (see Fig. 20). Thus, diffusion calculations confirm the diffusion theory of the graphite degradation skin.

It remains to explain the change in the thickness of the graphite degradation zone as a function of the metallostatic height (the edge effect for graphite degeneration) seen in Fig. 17. We propose that liquid convection in the solidifying metal determines the outcome, as follows. If high liquid convection occurs prior and during solidification, liquid rich in Mg is transported from the bulk into the surface layers of the casting and graphite degradation is minimal. However, if convection is low, liquid poor in Mg solidifies resulting in high graphite degradation. Indeed, for the particular casting configuration used in this research Magmasoft calculations suggest lower convection levels in the lower regions of the test sample because of the corner effects (Fig. 35).

### Graphite Depletion Rim

The cause for the graphite depletion rim must be carbon loss in the surface layer of the casting. Carbon loss is to be expected if there is an oxidizing atmosphere in the mold. This was indeed the case for resin bonded molds without carbonaceous additions used in this research. A carbon diffusion model similar to the one for magnesium discussed earlier was developed. The basic assumptions of the model included: 1) carbon sink at mold/metal interface (there is enough oxygen; oxygen – carbon reaction is instantaneous); 2) no liquid convection; 3) initial carbon content of 4.23%. The diffusivity of carbon in liquid iron was taken as  $2 \cdot 10^{-8}$  m<sup>2</sup>/s. The local solidification time calculated with the Magmasoft code for a DI plate having dimensions of 100x20x6mm was 18s.

The maximum solubility of carbon in austenite is 2.1%C for the Fe-C system at the eutectic temperature. Silicon decreases carbon solubility according to the relationship:

$$\Delta C_E^{Si} = -0.11 \cdot \%Si \quad (4)$$

where  $\Delta C_E^{Si}$  is the change in carbon solubility at point E (max. solubility of C in austenite) on the FeC diagram<sup>13</sup>. For 2.73%Si we calculate  $\Delta C_E^{Si} = 0.3\%$ , which gives a maximum solubility of 2.1 - 0.3 = 1.8%C. This is the minimum carbon content for graphite formation.

The results of the calculation are presented in Fig. 34b. It is seen that the carbon content decreases below 2.1%, which

is the maximum limit for graphite formation, at a distance of 0.2mm from the surface. Thus, the predicted carbon depletion layer is 0.2mm thick. The average measured graphite depletion rim for thin DI reported earlier in this paper is in the range of 0.15 to 0.45mm (see Fig. 20/Table 6). Thus, carbon diffusion calculations confirm the diffusion theory of the graphite depletion skin.

### Pearlitic rim

Let us now turn to the pearlite rim. Two different mechanisms can be responsible for its formation:

1. Carbon oxidation in the surface layer of the casting because of reaction with the mold atmosphere resulting in carbon depletion decreases the number of nuclei available for ferrite growth during the A1 transformation, and thus favors pearlite formation.
2. Carbon or sulfur diffusion from the mold into the surface layer of the casting favors pearlitic transformation in the skin during cooling through the A1 temperature.

The first mechanism has been confirmed in the previous section. A simple diffusion calculation can be performed to check the second mechanism. Assuming the solid diffusivity of C in austenite of the order of  $1.5 \cdot 10^{-10}$  m<sup>2</sup>/s, and taking a local transformation time of 500s, the diffusion distance is calculated to be:

$$L = \sqrt{D \cdot t} = 0.3 \text{ mm} \quad (5)$$

The average measured pearlitic rim is about 0.25mm (see Fig. 11).

Whether the carbon film on the surface of the advancing front of liquid cast iron reported in recent work<sup>14</sup> has any correlation to the casting skin is still to be explored.

### Acknowledgements

This work was made possible by a grant from the American Foundry Society, AFS Research Project 04-05#02. The authors are indebted to the members of the AFS 5I (Ductile and Compacted Graphite Iron Research) Committee and of the Project Steering Committee (Ron Walling, chair) for their support and many useful suggestions and comments. Stephanie Wills is grateful to Ashland Casting Solutions for the financial support during her Master of Sciences studies at OSU, and all authors are thankful for permission to use the Ashland casting laboratory. At the time the research was performed Dr. Juan Massone, permanently with the Univ. of Mar del Plata, Argentina, was a Fulbright Scholar at OSU.

## REFERENCES

1. G.M. Goodrich and R.W. Lobenhofer, "Effect of Cooling Rate on Ductile Iron Mechanical Properties", *AFS Transactions*, vol. 110 (2002) pp. 1003-1032.
2. F. Mampaey, P. Li and E. Wittink, "Variation of Gray Iron Strength Along the Casting Diameter", *AFS Transactions*, vol. 111 (2003) pp. 755-772.
3. J.W. Torrance and D.M. Stefanescu, "Investigation on the Effect of Surface Roughness on the Static Mechanical Properties of Thin-Wall Ductile Iron Castings", *AFS Transactions*, vol. 112 (2004) pp. 757-772.
4. L.P. Dix, R. Ruxanda, J. Torrance, M. Fukumoto and D.M. Stefanescu, "Static Mechanical Properties of Ferritic and Pearlitic", *AFS Transactions*, vol. 111 (2003) pp. 895-910.
5. C. Labrecque, M. Gagne, A. Javaid, and M. Sahoo, "Production and Properties of Thin-Wall Ductile Iron Castings", *International Journal of Cast Metals Research*, Vol. 16, Part 1/3 (2003) pp. 313-318.
6. R.C. Aufderheide, R.E. Showman and M.A. Hysell, "Controlling the "Skin Effect" on Thin-Wall Ductile Iron Castings", *AFS Transactions*, vol. 113 (2005) pp. 567-579.
7. F.C. Duncan and J. Kroker, "Difficulties in Controlling and Measuring Flake Skin in CGI", *WFO Technical Forum*, Dusseldorf, Germany (2007).
8. Azterlan, Euskadia, Spain, Private Communication.
9. C. Labrecque, M. Gagne, P. Cabanne, C. Francois, C. Becret, and F. Hoffman, "Comparative Study of Fatigue Endurance Limit For 4 and 6 MM Thin Wall Ductile Iron Castings", *International Journal of Metalcasting*, vol. 2, issue 2 (2008) pp.7-17.
10. D.M. Stefanescu and F.R. Juretzko, "Study of the Effect of Some Process Variables on the Surface Roughness and the Tensile Properties of Thin Wall Ductile Iron Castings", *AFS Transactions*, vol. 115 (2007) pp. 637-645.
11. R.E. Ruxanda, D.M. Stefanescu, T.S. Piwonka, "Microstructure Characterization of Ductile Thin Wall Iron Castings", *AFS Transactions*, vol. 110 (2002) pp. 1131-1147.
12. D.M. Stefanescu, Stephanie Collins and J. Massone, "Study of the Effect of the Casting Skin on the Tensile Properties of Light Weight Ductile Iron Castings" *AFS Report* (Jan. 2008).
13. D.M. Stefanescu, "Thermodynamic Properties of Iron-Base Alloys", *ASM Handbook, Vol. 15: Casting* (1988) pp.61-70.
14. A. Habibollahzadeh and J. Campbell, "Surface Films on Liquid Grey Cast Iron: A Study by SEM", *AFS Transactions*, vol. 111 (2003) pp. 675-684.



## Technical Review & Discussion

### Quantification of Casting Skin in Ductile and Compacted Graphite Irons and Its Effect on Tensile Properties

D. Stefanescu, S. Wills and J. Massone,  
The Ohio State University, Columbus, OH, USA  
Flavia Duncan, Ashland Casting Solutions,  
Dublin, OH, USA

**Reviewer:** The authors indicate that in their CGI analysis that even though three samples were available, only one was presented. Analysis of the three samples and the finding of similar results would have added some credibility.

**Authors:** *Regarding the CGI samples, only results on one sample are shown because the other ones are very similar. A statement to this effect was added to the text. There is no reason to present the same results three times. If the readers desire additional information, please consult the full report quoted in the reference section.*

**Reviewer:** It seems implausible to me to establish the skin thickness in the CGI by averaging the shape factor, aspect ratio and microhardness, especially when the charts are analyzed separately. The authors say the microhardness test results are questionable. This may affect the conclusion about skin thickness.

**Authors:** *We disagree with the reviewer. Shape factor and aspect ratio data are very convincing either independently (Fig. 18) or averaged (Fig. 20). Comparison with the picture in Fig. 17 supports the conclusions drawn from micrographic measurements. The microhardness is indeed unreliable and it is not suggested to use it for evaluation of the skin casting. The evaluation of the casting skin is based on measurements not calculations.*

**Reviewer:** The charge used is questionable. Why would they use CGI returns as 40% of the charge? If the CGI was made with titanium to control the structure, the Ti would likely be retained in the melt and could potentially affect the graphite structure.

**Authors:** *The CGI returns are coming from iron made with the SinterCast process and thus contain no titanium. It is quite normal to use 40% DI returns in ductile iron production. The CGI returns used in this study are similar to DI returns, as they have a low sulfur level because of the previous Mg treatment.*

**Reviewer:** The mold design was unusual to say the least. First the mold was tipped up at a 15 degree angle and then five levels were poured at one time. This resulted in a very difficult to understand metallostatic head variable that certainly confounded the results and conclusions.

**Authors:** *True. The reason for the tilting was to provide quiescent filling of the mold. The other issues have been addressed by the authors in the revised paper.*

**Reviewer:** All of the statistical analyses are reported partially, missing some of the results that would allow determination if there are statistical correlations. The correlation results shown don't look at the comparison desired—the effect of skin on properties. The correlations look at one variable, linear regressions, and there is not one that shows a strong correlation (except YS to UTS). Does this indicate that something is missing from the analysis or the data. Have the authors tried multiple regressions using all of the independent variables which may have provided a better correlation.

**Authors:** *The statistical analysis includes all independent variables affecting a particular dependent variable of interest. There is no point in presenting correlations between independent variables. Indeed, there are no strong correlations. This has been explained by the authors in the statement: "Because only one as-cast surface was used in these experiments, the  $R^2$  was very poor." Multiple regression would have of course given a better  $R^2$ . However, in this case this would have been a useless exercise as the regression equations are not meant for calculations at this point.*

**Reviewer:** The authors try to make a point that the machined tensile and yield strength are higher than that for the plates with one as cast surface. The problem is that the elongation is less for the machined parts which would not be expected if the surface skin and rough surface were removed, since stress concentrators were removed. This tells us that the main factor affecting tensile strength is something other than the surface—something in the metal (post inoculation?) or mold effects on the cooling rate? Something does not make sense here. Does this make the calculation of skin quality and mechanisms of skin formation less meaningful?

**Authors:** *Indeed the average data for elongation are higher for the un-machined than for the machined samples, and this is hard to explain. Note however, the higher limit for the machined samples. It is possible that defects not seen with the naked eye during sample examination after testing are responsible for this anomaly. The following statement was added in the text: "The results presented in this section are mostly semi quantitative because the "as-cast" test samples had in fact only one of four surfaces as-cast. A better test casting that will include more casting skin when tested "as-cast" should be designed." The authors strongly disagree with the reviewer comment that: "This makes the calculation of skin quality and mechanisms of skin formation less meaningful." The differences in strength between the machined and un-machined samples are conclusive. There is nothing in the reviewer comments to invalidate the model for the mechanism of skin formation.*

**Reviewer:** Is the scatter in the information influencing the significance of the findings? It seems to me that the results teach us something that is qualitative and that we are missing something quantitatively that can be reached if more thought is given to methods for producing samples that can be tested with the skin on.

**Authors:** *We agree with the reviewer. The current research is mostly semi quantitative because of the test casting inadequacy. A better test sample that has more skin should and will be designed as part of the continuation of this project. The following statement was added in section 5.4: "The results presented in this section are mostly semi quantitative because the "as-cast" test samples had in fact only one of four surfaces as-cast. A better test casting that will include more casting skin when tested "as-cast" should be designed.*